

CBET lolol

(Hopefully soon to be Dr.) Philip W. X. Moloney

IMPERIAL

June 2024

Submitted in partial fulfilment of the requirements for the degree of
Doctor of Philosophy of Imperial College London

Department of Physics
Imperial College London
Prince Consort Road
London SW7 2AZ

List of Acronyms

CBET Cross-Beam Energy Transfer

RTI Rayleigh–Taylor instability

IFAR In-Flight Aspect Ratio

1 Cylindrical Simulations to Study the Effect of Beam Radius in Direct-Drive

This chapter describes a cylindrical, direct-drive implosion simulation platform and corresponding ensemble of simulations that was developed to study the effect of the beam radius initial condition on OMEGA laser facility experiments. Although results from the cylindrical simulations do not have the same convergence properties of spherical implosions, much of the essential physics which is important to studying the effect of beam radius is preserved. The main benefit of the geometry is that a 2-D ray-trace can be used to model the lasers which yields several orders of magnitude speed up, compared to spherical 3-D implosions. The reduction in computational expense allows ensembles of Cross-Beam Energy Transfer (CBET) simulations to be performed, which would be exceedingly expensive for 3-D spherical calculations. Beam radius strongly effects CBET and therefore including a model for the interaction in computational studies is crucial.

The chapter begins with a review of the work which has been done to study the beam radius initial condition for direct-drive implosions, with an emphasis on the use of this parameter in statistical modelling of OMEGA campaigns. A description of the cylindrical platform is then provided, which includes a discussion of its advantages, weaknesses and applicability to current OMEGA experiments. The tuning procedure which was followed to obtain hydrodynamically similar implosions at different beam radii is then described. The main results of the chapter are then presented, which include calculations of the power deposition asymmetry both with and without CBET and an explanation of why CBET typically amplifies the asymmetry. CBET is also shown to introduce *modal flips* of the deposition in time. Stagnation state asymmetries of the hydrodynamic profiles are then studied for all implosions and these demonstrate that while increasing beam radius in the absence of CBET reduces beam mode asymmetries, the opposite behaviour is observed in the presence of CBET, although the exact relationship proves is complex. The chapter concludes with a summary of the work and suggestions of further work that could be undertaken using the same cylindrical platform.

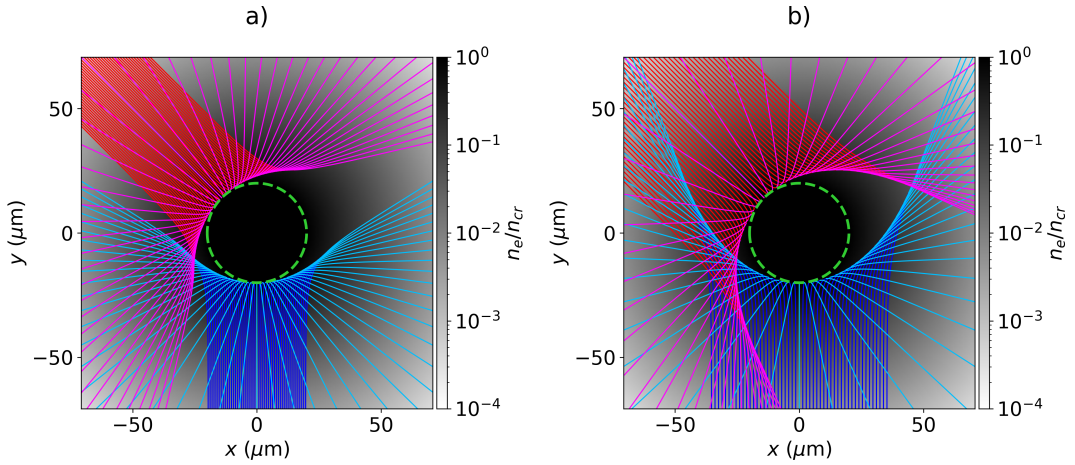


Figure 1.1: The trajectory of rays from two beams with Beam radii. The density profile for both simulations is $n_e = n_{cr} \exp [-(r_{\mu\text{m}} - 20)/100]$. Panels a) and b) plot rays from beams with widths $\sigma = 10$ and $18 \mu\text{m}$ respectively. Ray trajectories are separated for each beam by colour depending on their sheet. Red and dark blue rays are from the incident sheet (before the ray caustic) and magenta and light blue rays are from the reflected sheet (after the ray caustic).

1.1 Introduction to Beam Radius in Direct-Drive Inertial Confinement Fusion

An idealised direct drive implosion, (neglecting the effect of random or otherwise, shot-to-shot variations) has a limited number of initial conditions which define the implosion. The target can be described by a set of materials and their thicknesses. Initial target parameters are intimately coupled to the physics of the implosion and, in part, dictate the propagation time of shocks through the target, hydrodynamic stability and absorption of the laser energy. The pulse shape describes the laser power which is incident of the target as a function of time. This can be designed to, for example, drive shocks by introducing sharp rises in the incident power with time, which leads to sharp gradients in ablation pressure [1]. A given facility also has a number of beam ports each of which has a specific origin and pointing location, which influence the magnitude of the *beam mode* asymmetry, which arises from the uniformity of laser absorption. The intensity profile of each laser and specifically the beam radius is an additional parameter which can be varied and plays an important role in defining both the power which can be coupled to the target and the magnitude of beam mode asymmetry.

As shall be explored in this chapter, increasing the beam radius alters the magnitude of energy lost via CBET leading to a reduction in the maximum target mass that can be imploded at a given speed. The beam radius relative to the target is therefore often effectively varied from shot to shot by changing the outer radius (and therefore mass) of the target. This defines a dimensional variable, which is the radius of the beam divided by the target radius, R_b/R_t . Typically, at the OMEGA laser facility, this is explicitly defined as the radius of the beam

which contains 95 % of the incident power divided by the initial outer target radius [2–4],

$$R_b/R_t = \frac{r_{95}}{R_t}, \quad (1.1)$$

where r_{95} is defined by the integral,

$$\int_0^{r_{95}} e^{-|\frac{r}{\sigma}|^{n_s}} dr = 0.95, \quad (1.2)$$

and the definition of a circular, super-Gaussian beam profile from Eq. ?? has been used. In the absence of CBET it can intuitively be understood that increasing this parameter should improve the uniformity of the laser illumination, because beam spots overlap each other more on the target, and therefore reduce the beam mode [5]. Larger R_b/R_t also lead to slightly less absorption in the absence of CBET, because a larger fraction of the incident light (especially at late time as the target converges) would reach lower density plasma and therefore not be absorbed. CBET significantly complicates this interpretation, however.

Fig. 1.1.a and Fig. 1.1.b plot results of a ray tracing calculation with a direct-drive relevant, exponentially decaying plasma density with a smaller and larger beam respectively. In direct-drive, backscatter CBET is the dominant mechanism which depletes absorption, which is where outbound light gains energy from inbound light¹. The outward rays from the small beam radius simulation in Fig. 1.1.a do not overlap the incident light from the other beam and therefore limited CBET between these beams will occur. The trajectories from the larger radius simulation in Fig. 1.1.b, however do cross the inbound rays from the other beam, which could lead to a resonant CBET interaction, and significant reduction of the absorbed power. As was shown in Fig. ??, CBET also substantially increases absorption asymmetry on the OMEGA laser facility. This means that in the presence of CBET, the effect of increasing R_b/R_t on illumination asymmetry is not clear. While in the absence of CBET, it should lead to greater beam overlap, this increased overlap will result in more CBET which could reduce uniformity of absorption.

Isolating the contribution of CBET is of particular importance to allow extrapolation of experimental results to future facilities, because it is hoped that adding bandwidth to lasers will almost entirely eliminate CBET scattering. Studying which of these effects dominates is difficult to do experimentally, as significant backscatter CBET occurs at all laser facilities which are capable of conducting compression experiments. Therefore, computational studies are well suited to investigate how R_b/R_t influences performance and the role of CBET in this scaling.

1.1.1 Previous Work Studying the Effect of R_b/R_t on OMEGA

A great deal of experimental and computational work has been conducted to explore the effect that the beam radius has on direct-drive implosions. Froula et al. conducted a series of implosions which systematically varied R_b/R_t to explore the balance between increased

¹Note here that outbound here means light travelling quasi-parallel to the approximately radially outward fluid velocity and inbound means quasi-anti-parallel.

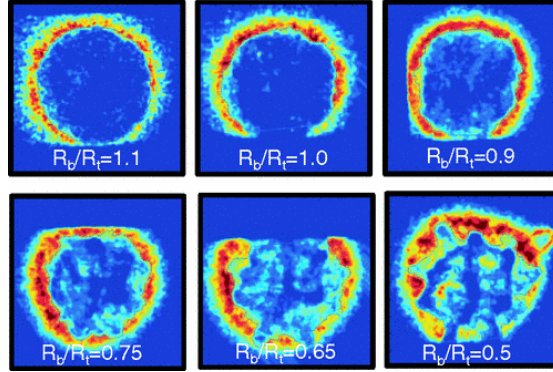


Figure 1.2: Soft x-rays emitted from the ablation surface of direct-drive implosions with various R_b/R_t values, as measured by an x-ray framing camera. All images are taken at a constant capsule radius of $R = 175 \mu\text{m}$. The figure has been reproduced with permission from Ref. [2].

CBET at larger beam radii, which reduced the coupled energy and increased illumination non-uniformity at lower radii [2]. Soft x-ray emission data from a selection of implosions with different radii are plotted in Fig. 1.2, all of which are taken at the same convergence shell radius of the target as it implodes inwards. These images show that at lower values of R_b/R_t , mid-mode perturbations² become increasingly significant. The results of these experiments found that neutron yield was maximised at $R_b/R_t \sim 0.8$. 1-D modelling using the CBET model in LILAC was in good agreement with the experimental results, verifying that CBET was responsible for the decrease in coupled energy to the target [6].

1.1.2 Statistical Modelling of OMEGA Direct-Drive Implosions

In recent years, a lot of work has been carried out to develop a statistical modelling capability for direct-drive implosions on the OMEGA laser facility. This modelling serves several critical purposes including enhancing the predictive capability of simulations [7], guiding experimental design to achieve higher performance implosions [8], identifying important sources of degradation on current facilities [5, 9] and validating simulation codes to help ensure they produce physically relevant results [10]. The first generation statistical model, described by Lees *et al.* in Ref. [7], created a mapping between experimental and 1-D simulation results in order to explain significant differences in their results. 1-D simulation results are fed into the model and degraded by a series of power law multiplications, which returns a more physically accurate experimental yield. Each power law multiplication represents a physical process for yield degradation with respect to 1-D physics, not included in the simulation. Each of these is termed a *yield over clean* (YOC_i), where the i refers to the different physical processes included in the model. The neutron yield from the 1-D simulation ($\text{Y}_{1\text{-D}}^{\text{sim}}$) can thus be converted to a prediction of the experimental yield [7],

$$\text{Y}^{\text{exp}} = (\text{YOC}_h \text{YOC}_f \text{YOC}_{\ell=1} \text{YOC}_b \text{YOC}_{\text{res}}) \text{Y}_{1\text{-D}}^{\text{sim}}, \quad (1.3)$$

²In direct-drive, *mid-modes* are loosely defined as modes similar to $\ell = 10$.

where YOC_h is a degradation term from hydrodynamics and instability growth, YOC_f is degradation due to radioactive decay of the Tritium fill, $\text{YOC}_{\ell=1}$ is degradation from $\ell = 1$ modes, YOC_b is degradation from finite number and radius of beams and YOC_{res} is a residual size scaling which is required to reduce performance of hydrodynamically downscaled implosions [11]. Each of these terms and their functional forms shall be discussed briefly, in order to provide context for the utility of the model and highlight that understanding the relevant physical processes which lead to degradation can improve its performance.

Hydrodynamic Degradation 1-D simulations do not capture short wavelength perturbations which grow via the Rayleigh–Taylor instability (RTI) and reduce the yield of experiments by puncturing and breaking up the shell as the capsule implodes inwards. Instabilities may be seeded by laser imprint or small scale defects in the target materials. Degradation can be reduced by altering implosion design to increase the shell adiabat which increases the ablative stabilisation of the RTI, or by lowering the In-Flight Aspect Ratio (IFAR), which increases the distance that the instability must grow through to puncture the shell. Scaling with the target convergence ratio, $C_R \equiv R_0/R_{\text{stag}}$, is included along with the ratio of outer to inner shell radius, $\hat{D} \equiv R_{\text{out}}/R_{\text{in}}$, which is believed to compensate for inaccuracies in modelling the shock propagation speed through the target. The hydrodynamic degradation term thus has the functional form,

$$\text{YOC}_h = \left[\frac{(\alpha/3)^{1.1}}{\text{IFAR}/20} \right]^{\mu_1} C_R^{\mu_2} \hat{D}^{\mu_3}, \quad (1.4)$$

where the μ_i fitting parameters, which are obtained from nonlinear regression across many OMEGA shots. The fitting procedure demonstrated that experimental yields are very significantly reduced by these hydrodynamic degradations, with the most unstable shots yielding values of $\text{YOC}_h \sim 0.1$ [5].

Fill Age Degradation OMEGA cryogenic implosions contain a DT fuel gas fill with a surrounding ice layer. The tritium in this fuel is unstable and undergoes radioactive decay to ${}^3\text{He}$ over the period of days to weeks which typically pass from initial gas filling to shot day [12]. ${}^3\text{He}$ has a lower freezing temperature than DT and thus sublimates, accumulating in the fill region. The accumulation of Helium in the gas reduces the final yield both by increasing radiative losses due to its higher ionisation, and by increasing density of the vapour, reducing compressibility and thus decreasing stagnation pressure in the hot-spot. Both of these effects can be captured by conducting 1-D simulations with a ${}^3\text{He}$ concentration (and corresponding reduction of tritium density) which is a function of fill age. The yield over clean due to the fill age and radioactive decay can then be taken as the ratio of these 1-D simulation yields,

$$\text{YOC}_h = \left(\frac{Y_{1\text{-D},\text{He}}^{\text{sim}}}{Y_{1\text{-D}}^{\text{sim}}} \right)^{\mu_4}, \quad (1.5)$$

where $Y_{1\text{-D},\text{He}}^{\text{sim}}$ is the yield from the 1-D simulation with accumulated ${}^3\text{He}$ and μ_4 is a fitting parameter. Good agreement is observed with a fitted parameter value of $\mu_4 = 1.3$. The

value is larger than 1 (and the 95 % confidence interval does not include 1), which suggests stronger degradation than observed in 1-D calculations. This could be due to radioactive decay damaging the shell and leading to hydrodynamic instability growth [5].

Mode 1 Degradation In direct-drive implosions on the OMEGA facility, $\ell = 1$ modes can be introduced to an implosion by a global offset of the target from the target chamber centre, mispointing of the laser beams or a power imbalance. These are random and uncontrollable and therefore the statistical models can only account for their effect after the shot has occurred, returning an estimated yield which could have been achieved if no $\ell = 1$ were present, $Y^{\text{exp}}/\text{YOC}_{\ell=1}$. Mode 1 asymmetries have a clear signature in the broadening of the neutron time-of-flight detector peaks, when observed from orthogonal lines of sight. The width of the peaks from multiple lines of sight can be analysed to return an angularly resolved apparent ion temperature map [13], the asymmetry of which is dominated by the lowest mode of the hot-spot [14]. Thus, it is deduced that the ratio of the maximum to minimum apparent ion temperatures from the experimental neutron time-of-flight signal can be used as a proxy for the amplitude of the mode 1, $R_T = T_{\max}/T_{\min}$. This leads to a yield over clean expression for the $\ell = 1$ degradation source,

$$\begin{aligned} \text{YOC}_{\ell=1} &= \hat{R}_T^{\mu_5}, \\ \hat{R}_t &\equiv \max \left(\frac{R_T}{R_T^{\min}} \right), \end{aligned} \quad (1.6)$$

where μ_5 is the fitting parameter and the minimum threshold value, R_T^{\min} is introduced due to imperfect reconstruction of the apparent ion temperature map and fitted separately. Work has been conducted to minimise the effect of the $\ell = 1$ on OMEGA by repositioning the target after several initial shots to minimise the asymmetry in the apparent ion temperature measurement and thus increase performance [13].

Finite Beam Degradation The OMEGA laser facility has 60 beams arranged around a sphere which gives generally good illumination uniformity on a hard sphere surface, less than the 1 % deviation which is believed to be necessary to achieve ignition [15, 16]. An $\ell = 10$ remains in the deposition however, as is demonstrated in Fig. ??, which is often referred to as the beam-mode. In the absence of CBET, increasing R_b/R_t increases the hard-sphere illumination uniformity [9]. As already described however, increasing beam radius allows leads to more blowby light and therefore more CBET. This reduces the coupled energy and potentially introduces additional asymmetry to the implosion. Additionally, increasing the overlap of beams on the target could reduce the amplitude of the imprint seed and therefore increase performance. The uncertainty as to which physical mechanisms are important, is

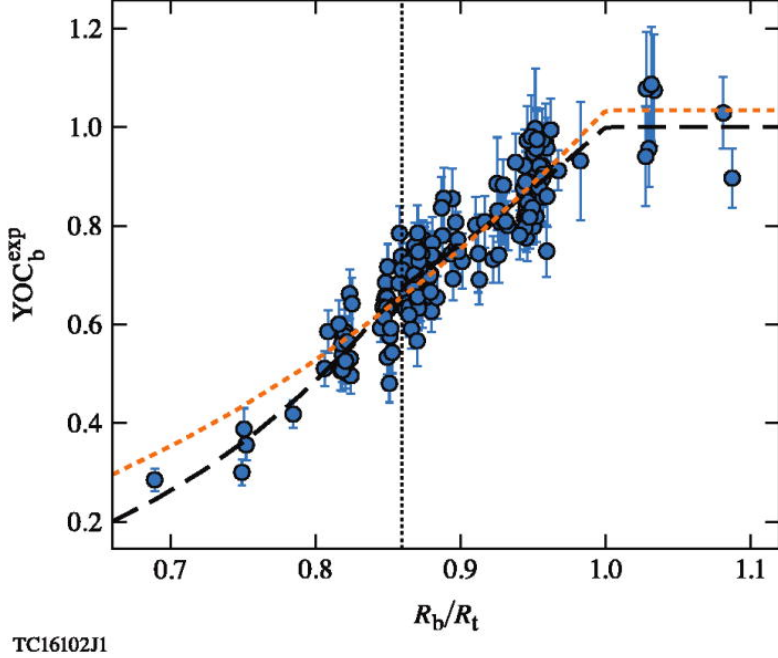


Figure 1.3: Experimentally inferred fusion yield degradation due to the finite beam source on the OMEGA laser facility. The dotted orange curve is the fit obtained from just using the $\bar{R}_{b/t}$ relation, while the black dashed curve uses the full relation in Eq. 1.7. The vertical dotted line indicates the critical threshold, $\hat{R}_{b/t}^{\text{crit}} = 0.86$, after which the $\hat{R}_{b/t}$ also has an effect. The cross validation error from the $\bar{R}_{b/t}$ and full fit is -1.0% and -0.5% respectively. The figure has been reproduced with permission from Ref. [5].

highlighted by the complexity of the degradation parameter,

$$\begin{aligned}
 YOC_b &= \left(\bar{R}_{b/t} \right)^{\mu_6} \left(\hat{R}_{b/t} \right)^{\mu_7}, \\
 \bar{R}_{b/t} &= \begin{cases} R_b/R_t & \text{if } R_b < R_t, \\ 1 & \text{if } R_b \geq R_t, \end{cases} \\
 \hat{R}_{b/t} &= \begin{cases} \frac{R_b}{R_t R_{b/t}^{\text{crit}}} & \text{if } R_b/R_t < R_{b/t}^{\text{crit}}, \\ 1 & \text{if } R_b/R_t \geq R_{b/t}^{\text{crit}}, \end{cases}
 \end{aligned} \tag{1.7}$$

where μ_6 & μ_7 are fitting parameters, the threshold behaviour in $\bar{R}_{b/t}$ was chosen to fit a small number of shots (< 10) at $R_b/R_t > 1$ and the threshold behaviour at $R_{b/t}^{\text{crit}}$ was introduced to fit a physically unexplained transition between two regimes in the data.

The fitted curve from the model is shown in Fig. 1.3, as the black dashed curve alongside the inferred values from experimental data points. Also plotted in orange is a fitted curve obtained from just using the simple $\bar{R}_{b/t}$ degradation. Introducing the $R_{b/t}^{\text{crit}}$ threshold significantly reduces the cross validation error of the fit. The switch between the two regimes is found from the fitting procedure to occur at $R_{b/t}^{\text{crit}} = 0.86$. This is close to value of minimum illumination asymmetry for beams incident on a hard hard-sphere ($R_b/R_t = 0.82$), which suggests that the degradation at the lowest values of R_b/R_t is dominated by beam-

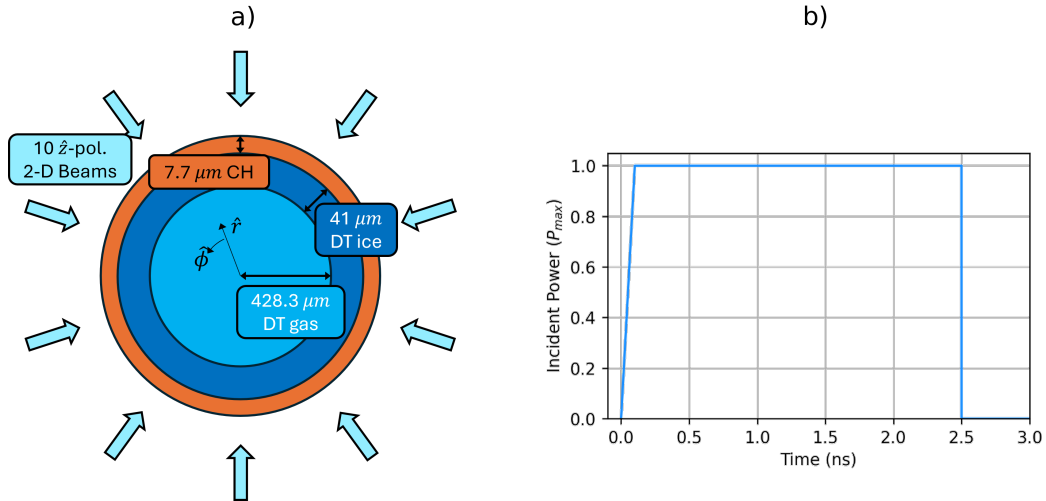


Figure 1.4: The target initial conditions with beam geometry, a), and pulse shape, b), used for the 2-D cylindrical simulations. All beams were polarised out of the simulation plane, in the $+\hat{z}$ direction. Initial layer radii were taken from the initial conditions for OMEGA shot 89224, presented in Fig. ??a.

mode, however this has not been experimentally or computationally verified. Experiments between $R_{b/t}^{\text{crit}} < R_b/R_t < 1$ could be influenced by changing behaviour due to CBET or imprint, which is not properly captured by the 1-D LILAC simulations included in the model.

The hypothesis tested in this chapter is that the change in yield over clean at $R_b/R_t = R_{b/t}^{\text{crit}}$ is due to increasing CBET as beam radius increases, which increases beam mode asymmetry and therefore suppresses the YOC_b term. Although LILAC does include a model for CBET, it is a 1-D code and therefore the 3-D beam mode perturbations cannot be inferred from its results. Qualitatively, this hypothesis can explain the observed behaviour in Fig. 1.3, which demonstrates that at $R_{b/t}^{\text{crit}}$, the gradient of YOC_b decreases. This behaviour should occur if CBET acted to amplify the asymmetry of the stagnation state, causing the simulation to be less similar to the 1-D LILAC results.

Table 1.1: Results of the 1-D Tuning Simulations.

R_b/R_t		P_{\max} (TW/cm)	I_0 (10^{14} W/cm 2)	t_{bang} (ns)	Y_{DT} (10^{13} /cm)
0.75	No CBET	54.44	0.85	2.49	1.53
	CBET			2.51	1.44
0.80	No CBET	58.25	0.83	2.49	1.56
	CBET			2.51	1.45
0.85	No CBET	63.44	0.83	2.48	1.67
	CBET			2.51	1.43
0.90	No CBET	70.00	0.85	2.47	1.82
	CBET			2.50	1.41
0.95	No CBET	77.94	0.89	2.46	1.99
	CBET			2.49	1.49
1.00	No CBET	87.25	0.93	2.45	2.15
	CBET			2.49	1.60
1.05	No CBET	97.94	0.99	2.46	2.27
	CBET			2.50	1.61
1.10	No CBET	110.00	1.06	2.47	2.31
	CBET			2.51	1.52

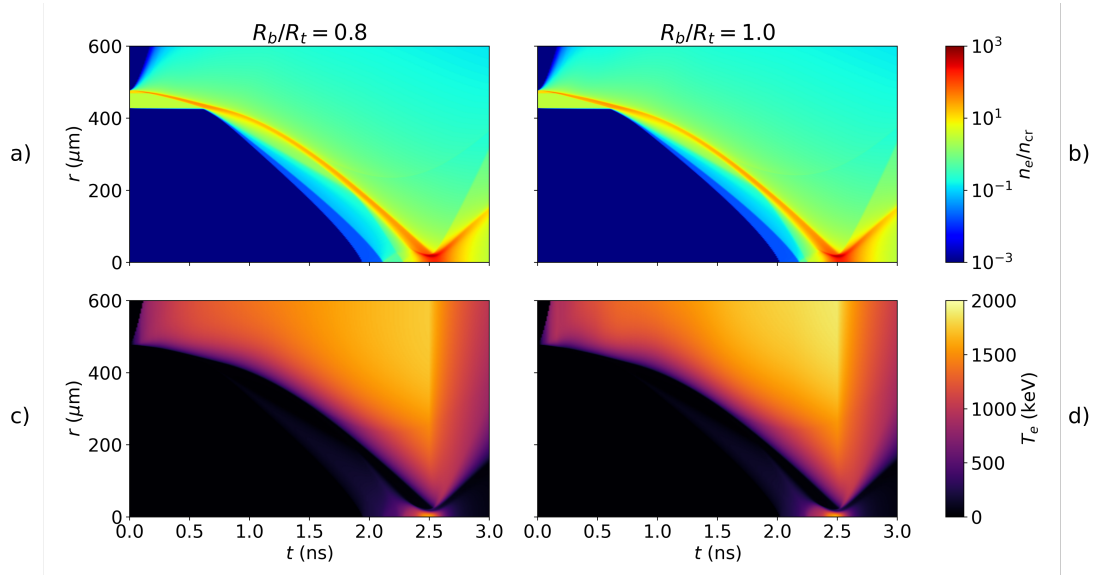


Figure 1.5: Streak plots from two of the 1-D tuning simulations. Panels a) & b) plot the electron density as a function of time (x-axis) and radius (y-axis) for the CBET simulations of the $R_b/R_t = 0.8$ & $R_b/R_t = 1.0$ simulations respectively. Panels c) & d) plot the same but electron temperature for the $R_b/R_t = 0.8$ & $R_b/R_t = 1.0$ simulations respectively.

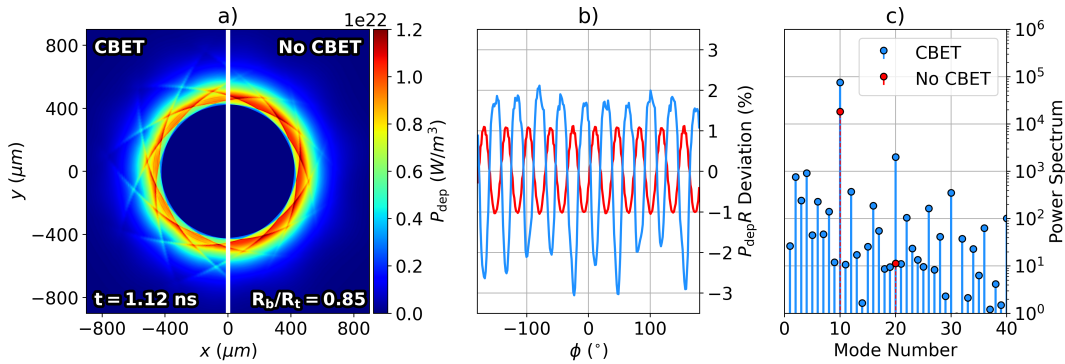


Figure 1.6: This figure demonstrates the analysis workflow to obtain the key results for this chapter. The power deposition at $t = 1.12 \text{ ns}$ from the CBET (left) and no CBET (right) simulations are plotted in panel a) for the $R_b/R_t = 0.85$ case. Panel b) plots the radially integrated deposition from the profiles in a) as a function of azimuthal angle. It can be seen from this plot, that the CBET asymmetry (light-blue) is greater than the no CBET asymmetry (red). The power spectrum of these profiles is then plotted in panel c). This demonstrates that the dominant modes in the spectrum are multiples of the number of beams.

1.2 Cylindrical Simulation Platform for Beam Radius Parameter Scan

1.2.1 Assumptions and Validity of the Cylindrical Simulation Platform

1.2.2 Problems with Traditional Methods of Investigating Beam Radius Parameter Computationally

1.2.3 Pulse Shape and Target Initial Conditions

1.2.4 1-D Implosion Tuning

1.3 CBET Induced Modal Flips in Power Deposition Asymmetries

1.3.1 Analysis and Quantity Definitions

1.3.2 Deposition Asymmetries in the Absence of CBET

1.3.3 CBET Imprint on Incident Field

1.3.4 Modal Flips of Power Deposition Asymmetries

1.4 Stagnation State Asymmetry

1.4.1 Hotspot Profiles

1.4.2 Stagnation State Asymmetry Trend with Beam Radius

1.4.3 Time Resolved Asymmetry Growth

1.5 Conclusions

1.5.1 Summary of work

1.5.2 Future Work

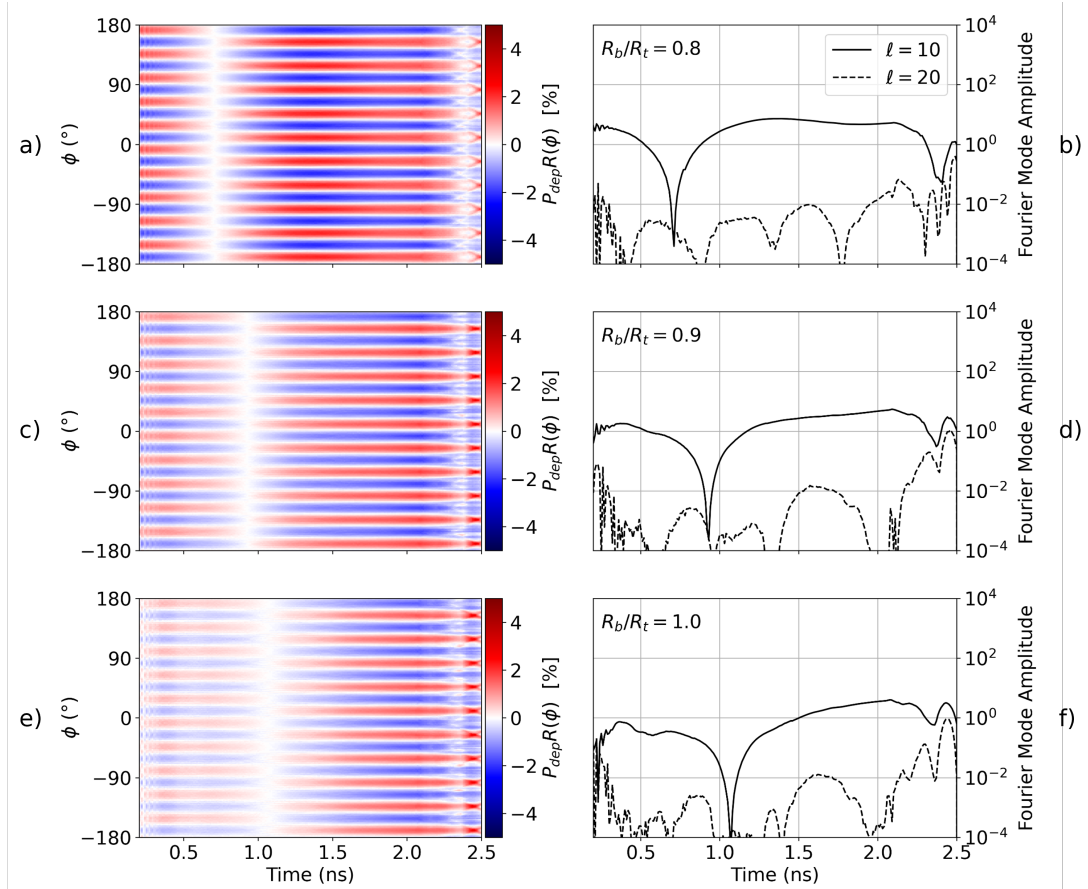


Figure 1.7: This figure plots the radially integrated deposited power from no CBET simulations as a function of time (x -axis) and angle (y -axis), alongside amplitudes of the dominant modes from a Fourier power spectrum. Panels a) and b) plot the radially integrated deposited power and Fourier modes respectively for the $R_b/R_t = 0.8$ simulation. The same is plotted for the $R_b/R_t = 0.9$ simulation in c) & d) and for the $R_b/R_t = 1.0$ simulation in e) & f). The mode 10 from the number of beams is clearly visible in the radially integrated power plots as 10 peaks to troughs in angle at a given time, *i.e.* 10 cyclical perturbations along a vertical lineout.

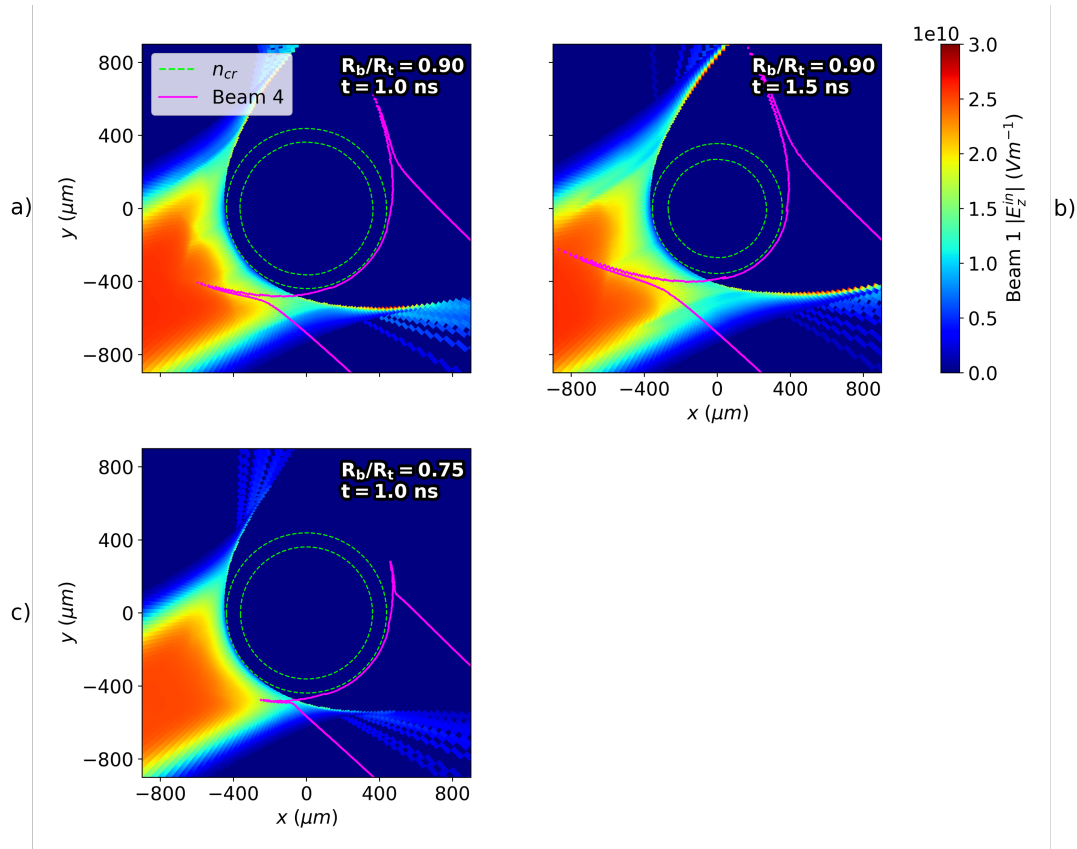


Figure 1.8: This plot illustrates the origin of the CBET induced asymmetry on power deposition and its dependence on R_b/R_t and target convergence. Each panel plots the incident field (including the effect of CBET), along with contours of the critical electron density and the $|E_z^{in}| = 1 \times 10^{10} \text{ Vm}^{-1}$ contour of another beam. Panel a) & b) plot this for the $R_b/R_t = 0.9$ simulation at $t = 1.0$ ns & $t = 1.5$ ns respectively. The convergence of the target in this time interval leads to greater convergence and therefore a change in the spatial location across the beam of the resonant CBET interaction. Panel c) plots the $R_b/R_t = 0.75$ at the same time as panel a). This demonstrates that the $R_b/R_t = 0.75$ beam is not wide enough at this time to lead to a resonant CBET interaction, unlike the wider beam in panel a).

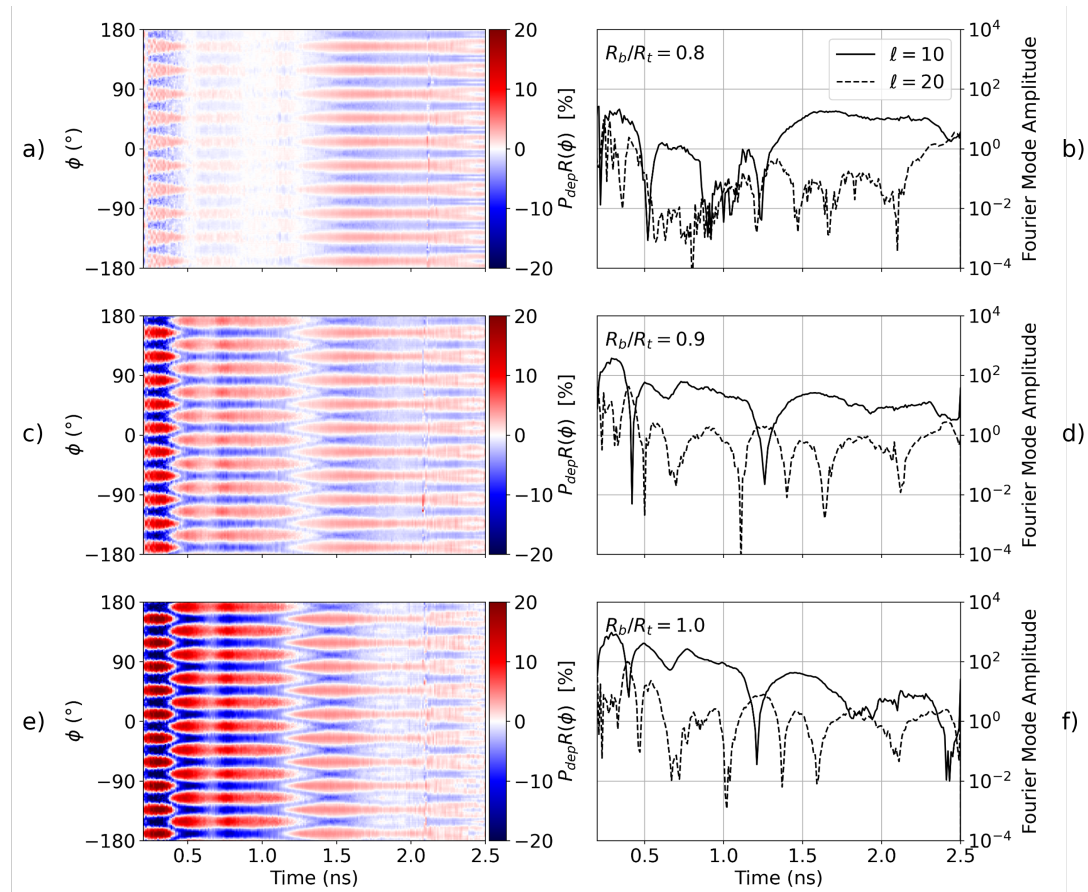


Figure 1.9: This figure plots the same as Fig. 1.7, but now for the equivalent simulation including the effect of CBET. Comparing these results and those in Fig. 1.7 demonstrates that CBET introduces additional modal-flips of the deposition and amplifies the magnitude of asymmetries.

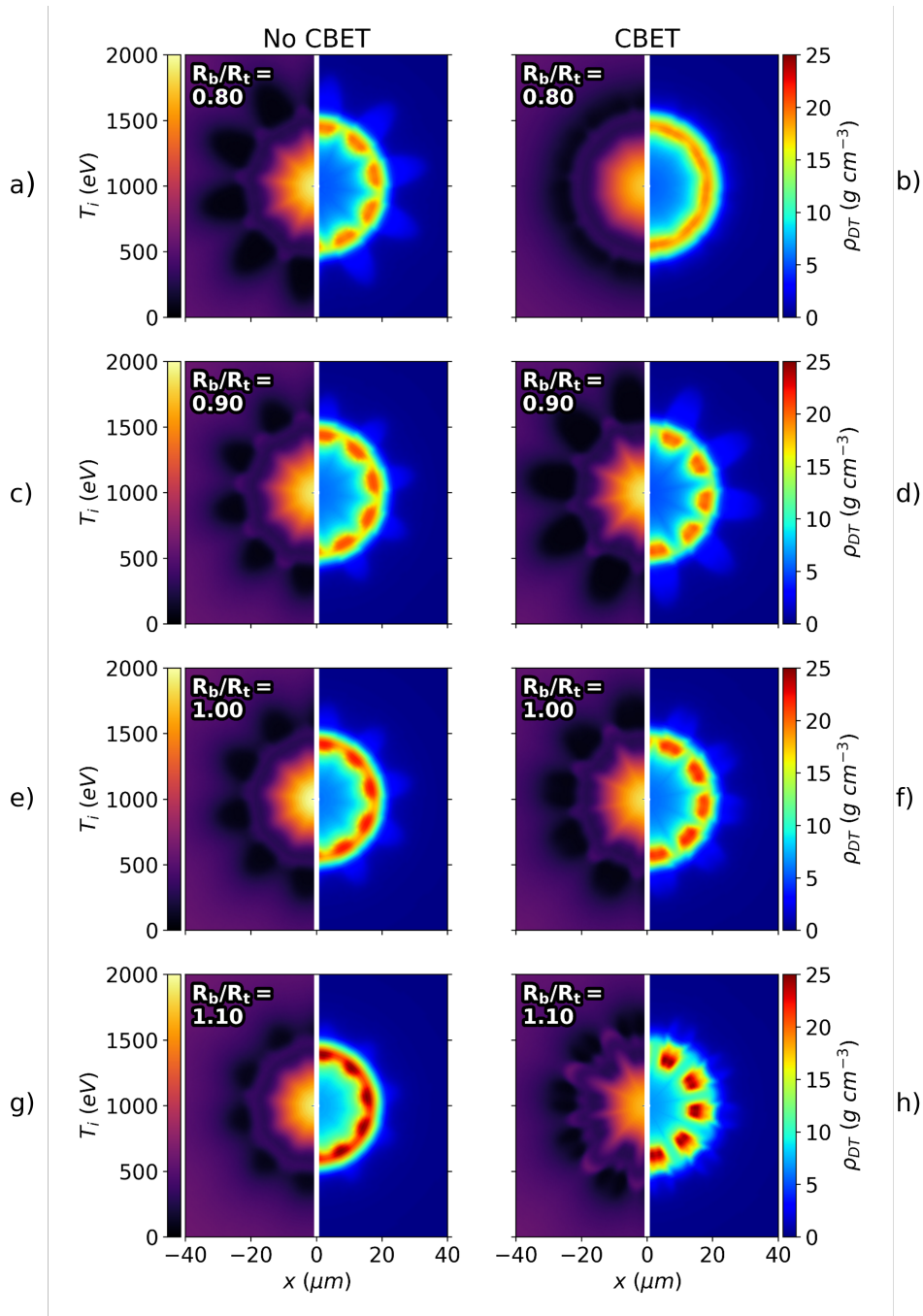


Figure 1.10: Densities of the DT fuel and ion temperatures for various R_b/R_t simulations both with and without CBET. Each row corresponds to a different R_b/R_t value; the left column contains simulations without CBET; and the right column contains simulations with CBET. It is visible from the density plots that increasing R_b/R_t improves stagnation symmetry for the no CBET simulations, but degrades it for the CBET simulations.

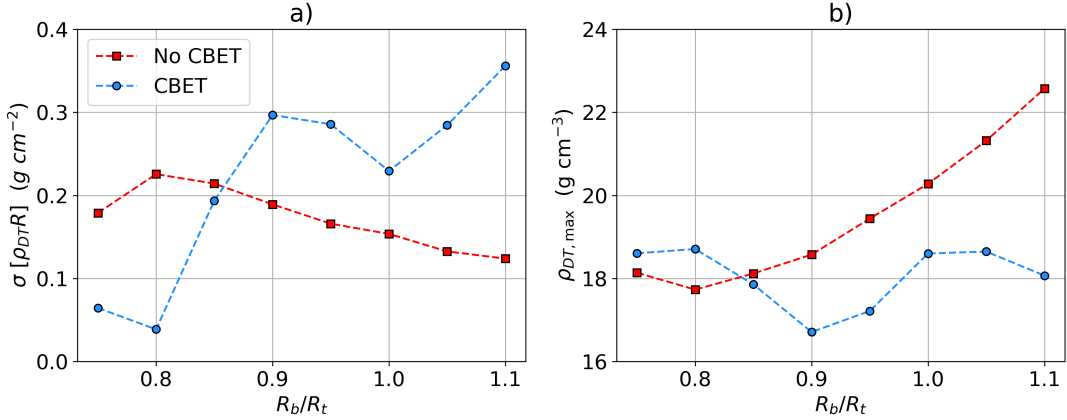


Figure 1.11: Trends of a) stagnation asymmetry and b) maximum (azimuthally averaged) fuel density for CBET and no CBET simulations. The no CBET improvement in symmetry with R_b/R_t is observed which also corresponds to improved compression. The symmetry trend including CBET is more complex, but broadly the stagnation state symmetry is worse with increasing R_b/R_t .

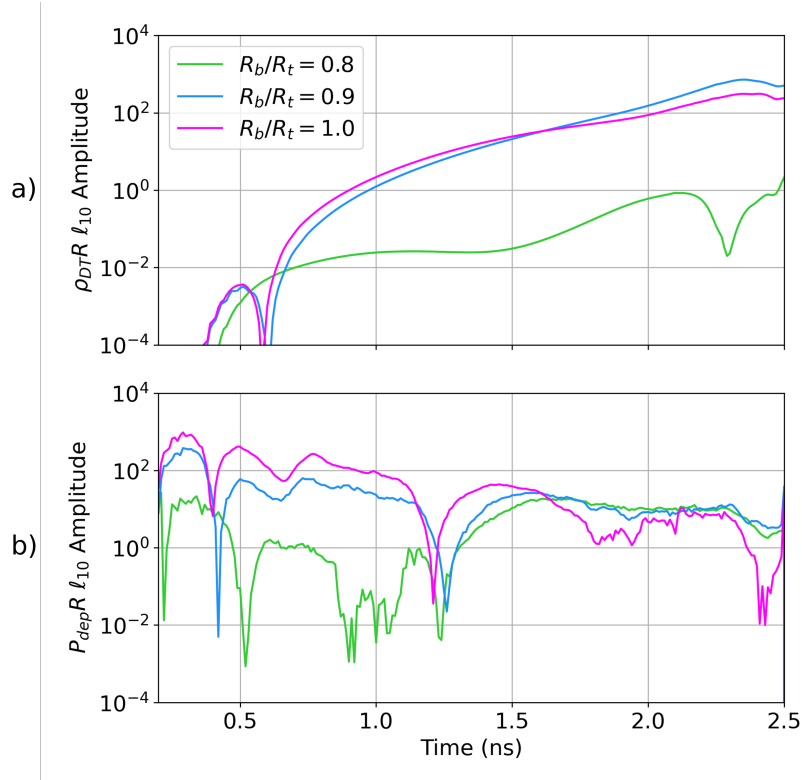


Figure 1.12: Time resolved $\ell = 10$ Fourier power spectrum amplitude for a) $\rho_{DT}R$ and b) $P_{dep}R$ for CBET simulations with 3 R_b/R_t values. The developing but unrealised modal flip for $R_b/R_t = 0.8$ from $t \sim 0.5 \rightarrow 1.2$ ns reduces the $P_{dep}R_{\ell=10}$ leading to slow $\rho_{DT}R_{\ell=10}$ growth and ultimately a relatively symmetric stagnation state. Despite large values of $\rho_{DT}R_{\ell=10}$ initially, the developing modal flip of the $R_b/R_t = 1.0$ simulation from $t \sim 1.8 \rightarrow 2.1$ ns slows the density asymmetry growth.

Appendices

A Numerics Appendices

Bibliography

- [1] R. H. H. Scott, D. Barlow, W. Trickey, A. Ruocco, K. Glize, L. Antonelli, M. Khan, and N. C. Woolsey. Shock-Augmented Ignition Approach to Laser Inertial Fusion. *Physical Review Letters*, 129(19):195001, November 2022. ISSN 0031-9007, 1079-7114. doi: 10.1103/PhysRevLett.129.195001. URL <https://link.aps.org/doi/10.1103/PhysRevLett.129.195001>. 6
- [2] D. H. Froula, I. V. Igumenshchev, D. T. Michel, D. H. Edgell, R. Follett, V. Yu. Glebov, V. N. Goncharov, J. Kwiatkowski, F. J. Marshall, P. B. Radha, W. Seka, C. Sorce, S. Stagnitto, C. Stoeckl, and T. C. Sangster. Increasing Hydrodynamic Efficiency by Reducing Cross-Beam Energy Transfer in Direct-Drive-Implosion Experiments. *Physical Review Letters*, 108(12):125003, March 2012. ISSN 0031-9007, 1079-7114. doi: 10.1103/PhysRevLett.108.125003. URL <https://link.aps.org/doi/10.1103/PhysRevLett.108.125003>. 7, 8
- [3] A. Colaïtis, R. K. Follett, C. Dorner, A. G. Seaton, D. Viala, I. Igumenshchev, D. Turnbull, V. Goncharov, and D. H. Froula. Exploration of cross-beam energy transfer mitigation constraints for designing an ignition-scale direct-drive inertial confinement fusion driver. *Physics of Plasmas*, 30(8):082701, August 2023. ISSN 1070-664X, 1089-7674. doi: 10.1063/5.0150813. URL <https://pubs.aip.org/pop/article/30/8/082701/2906541/Exploration-of-cross-beam-energy-transfer>.
- [4] K. S. Anderson, J. A. Marozas, T. J. B. Collins, C. J. Forrest, V. N. Goncharov, and D. Cao. Enhanced sensitivity to target offset when using cross-beam energy transfer mitigation techniques in direct-drive inertial confinement fusion implosions. *Physics of Plasmas*, 31(3):032704, March 2024. ISSN 1070-664X, 1089-7674. doi: 10.1063/5.0191277. URL <https://pubs.aip.org/pop/article/31/3/032704/3278248/Enhanced-sensitivity-to-target-offset-when-using>. 7
- [5] A. Lees, R. Betti, J. P. Knauer, V. Gopalaswamy, D. Patel, K. M. Woo, K. S. Anderson, E. M. Campbell, D. Cao, J. Carroll-Nellenback, R. Epstein, C. J. Forrest, V. N. Goncharov, D. R. Harding, S. X. Hu, I. V. Igumenshchev, R. T. Janezic, O. M. Manzion, P. B. Radha, S. P. Regan, A. Shvydky, R. C. Shah, W. T. Shmayda, C. Stoeckl, W. Theobald, and C. A. Thomas. Understanding the fusion yield dependencies in OMEGA DT-layered implosion experiments using a physics-based statistical mapping model. *Physics of Plasmas*, 30(1):012709, January 2023. ISSN 1070-664X, 1089-7674. doi: 10.1063/5.0106515. URL <https://pubs.aip.org/pop/article/30/1/012709/2867741/Understanding-the-fusion-yield-dependencies-in>. 7, 8, 9, 10, 11

- [6] I. V. Igumenshchev, W. Seka, D. H. Edgell, D. T. Michel, D. H. Froula, V. N. Goncharov, R. S. Craxton, L. Divol, R. Epstein, R. Follett, J. H. Kelly, T. Z. Kosc, A. V. Maximov, R. L. McCrory, D. D. Meyerhofer, P. Michel, J. F. Myatt, T. C. Sangster, A. Shvydky, S. Skupsky, and C. Stoeckl. Crossed-beam energy transfer in direct-drive implosions. *Physics of Plasmas*, 19(5):056314, May 2012. ISSN 1070-664X, 1089-7674. doi: 10.1063/1.4718594. URL <https://pubs.aip.org/pop/article/19/5/056314/596972/Crossed-beam-energy-transfer-in-direct-drive>. 8
- [7] A. Lees, R. Betti, J. P. Knauer, V. Gopalaswamy, D. Patel, K. M. Woo, K. S. Anderson, E. M. Campbell, D. Cao, J. Carroll-Nellenback, R. Epstein, C. Forrest, V. N. Goncharov, D. R. Harding, S. X. Hu, I. V. Igumenshchev, R. T. Janezic, O. M. Mannion, P. B. Radha, S. P. Regan, A. Shvydky, R. C. Shah, W. T. Shmyda, C. Stoeckl, W. Theobald, and C. Thomas. Experimentally Inferred Fusion Yield Dependencies of OMEGA Inertial Confinement Fusion Implosions. *Physical Review Letters*, 127(10):105001, August 2021. ISSN 0031-9007, 1079-7114. doi: 10.1103/PhysRevLett.127.105001. URL <https://link.aps.org/doi/10.1103/PhysRevLett.127.105001>. 8
- [8] V. Gopalaswamy, R. Betti, J. P. Knauer, N. Luciani, D. Patel, K. M. Woo, A. Bose, I. V. Igumenshchev, E. M. Campbell, K. S. Anderson, K. A. Bauer, M. J. Bonino, D. Cao, A. R. Christopherson, G. W. Collins, T. J. B. Collins, J. R. Davies, J. A. Delettrez, D. H. Edgell, R. Epstein, C. J. Forrest, D. H. Froula, V. Y. Glebov, V. N. Goncharov, D. R. Harding, S. X. Hu, D. W. Jacobs-Perkins, R. T. Janezic, J. H. Kelly, O. M. Mannion, A. Maximov, F. J. Marshall, D. T. Michel, S. Miller, S. F. B. Morse, J. Palastro, J. Peebles, P. B. Radha, S. P. Regan, S. Sampat, T. C. Sangster, A. B. Sefkow, W. Seka, R. C. Shah, W. T. Shmyda, A. Shvydky, C. Stoeckl, A. A. Solodov, W. Theobald, J. D. Zuegel, M. Gatu Johnson, R. D. Petrasso, C. K. Li, and J. A. Frenje. Tripled yield in direct-drive laser fusion through statistical modelling. *Nature*, 565(7741):581–586, January 2019. ISSN 0028-0836, 1476-4687. doi: 10.1038/s41586-019-0877-0. URL <https://www.nature.com/articles/s41586-019-0877-0>. 8
- [9] V. Gopalaswamy, R. Betti, J. P. Knauer, A. Lees, D. Patel, A. R. Christopherson, I. V. Igumenshchev, D. Cao, K. S. Anderson, A. Shvydky, D. H. Edgell, O. M. Mannion, C. Thomas, W. Theobald, C. Stoeckl, S. P. Regan, V. N. Goncharov, R. Shah, and E. M. Campbell. Using statistical modeling to predict and understand fusion experiments. *Physics of Plasmas*, 28(12):122705, December 2021. ISSN 1070-664X, 1089-7674. doi: 10.1063/5.0056662. URL <https://pubs.aip.org/pop/article/28/12/122705/108236/Using-statistical-modeling-to-predict-and>. 8, 10
- [10] R. Ejaz, V. Gopalaswamy, A. Lees, C. Kanan, D. Cao, and R. Betti. Deep learning-based predictive models for laser direct drive at the Omega Laser Facility. *Physics of Plasmas*, 31(5):052703, May 2024. ISSN 1070-664X, 1089-7674. doi: 10.1063/5.0195675. URL <https://pubs.aip.org/pop/article/31/5/052703/3293889/Deep-learning-based-predictive-models-for-laser>. 8

- [11] C. A. Thomas, D. Cao, W. Theobald, R. Betti, K. A. Anderson, K. A. Bauer, E. M. Campbell, A. R. Christopherson, T. J. B. Collins, R. S. Craxton, D. H. Edgell, R. Epstein, C. J. Forrest, V. Yu. Glebov, V. Gopalaswamy, I. V. Igumenshchev, S. T. Ivancic, D. W. Jacobs-Perkins, R. T. Janezic, T. Joshi, J. P. Knauer, J. Kwiatkowski, A. Lees, O. M. Mannion, F. J. Marshall, and LLE Team. Quantifying the Effects of Scale and Illumination Geometry in Laser Direct Drive. 2020:BO09.014, January 2020. URL <https://ui.adsabs.harvard.edu/abs/2020APS..DPPB09014T>. Conference Name: APS Division of Plasma Physics Meeting Abstracts ADS Bibcode: 2020APS..DPPB09014T. 9
- [12] S.P. Regan, V.N. Goncharov, T.C. Sangster, E.M. Campbell, R. Betti, J.W. Bates, K. Bauer, T. Bernat, S. Bhandarkar, T.R. Boehly, M.J. Bonino, A. Bose, D. Cao, L. Carlson, R. Chapman, T. Chapman, G.W. Collins, T.J.B. Collins, R.S. Craxton, J.A. Delettrez, D.H. Edgell, R. Epstein, M. Farrell, C.J. Forrest, R.K. Follett, J.A. Frenje, D.H. Froula, M. Gatu Johnson, C.R. Gibson, L. Gonzalez, C. Goyon, V.Yu Glebov, V. Gopalaswamy, A. Greenwood, D.R. Harding, M. Hohenberger, S.X. Hu, H. Huang, J. Hund, I.V. Igumenshchev, D.W. Jacobs-Perkins, R.T. Janezic, M. Karasik, J.H. Kelly, T.J. Kessler, J.P. Knauer, T.Z. Kosc, R. Luo, S.J. Loucks, J.A. Marozas, F.J. Marshall, M. Mauldin, R.L. McCrory, P.W. Mckenty, D.T. Michel, P. Michel, J.D. Moody, J.F. Myatt, A. Nikroo, P.M. Nilson, S.P. Obenschain, J.P. Palastro, J. Peebles, R.D. Petrasso, N. Petta, P.B. Radha, J.E. Ralph, M.J. Rosenberg, S. Sampat, A.J. Schmitt, M.J. Schmitt, M. Schoff, W. Seka, R. Shah, J.R. Rygg, J.G. Shaw, R. Short, W.T. Shmayda, M.J. Shoup, A. Shvydky, A.A. Solodov, C. Sorce, M. Stadermann, C. Stoeckl, W. Sweet, C. Taylor, R. Taylor, W. Theobald, D.P. Turnbull, J. Ulreich, M.D. Wittman, K.M. Woo, K. Youngblood, and J.D. Zuegel. The National Direct-Drive Inertial Confinement Fusion Program. *Nuclear Fusion*, 59(3):032007, March 2019. ISSN 0029-5515, 1741-4326. doi: 10.1088/1741-4326/aae9b5. URL <https://iopscience.iop.org/article/10.1088/1741-4326/aae9b5>. 9
- [13] O. M. Mannion, I. V. Igumenshchev, K. S. Anderson, R. Betti, E. M. Campbell, D. Cao, C. J. Forrest, M. Gatu Johnson, V. Yu. Glebov, V. N. Goncharov, V. Gopalaswamy, S. T. Ivancic, D. W. Jacobs-Perkins, A. Kalb, J. P. Knauer, J. Kwiatkowski, A. Lees, F. J. Marshall, M. Michalko, Z. L. Mohamed, D. Patel, H. G. Rinderknecht, R. C. Shah, C. Stoeckl, W. Theobald, K. M. Woo, and S. P. Regan. Mitigation of mode-one asymmetry in laser-direct-drive inertial confinement fusion implosions. *Physics of Plasmas*, 28(4):042701, April 2021. ISSN 1070-664X, 1089-7674. doi: 10.1063/5.0041554. URL <https://pubs.aip.org/pop/article/28/4/042701/263531/Mitigation-of-mode-one-asymmetry-in-laser-direct>. 10
- [14] K. M. Woo, R. Betti, O. M. Mannion, C. J. Forrest, J. P. Knauer, V. N. Goncharov, P. B. Radha, D. Patel, V. Gopalaswamy, and V. Yu. Glebov. Inferring thermal ion temperature and residual kinetic energy from nuclear measurements in inertial confinement fusion implosions. *Physics of Plasmas*, 27(6):062702, June 2020. ISSN 1070-664X, 1089-7674. doi: 10.1063/1.5144460. URL <https://pubs.aip.org/pop/article/27/6/062702/1025468/Inferring-thermal-ion-temperature-and-residual>. 10

-
- [15] R. S. Craxton, K. S. Anderson, T. R. Boehly, V. N. Goncharov, D. R. Harding, J. P. Knauer, R. L. McCrory, P. W. McKenty, D. D. Meyerhofer, J. F. Myatt, A. J. Schmitt, J. D. Sethian, R. W. Short, S. Skupsky, W. Theobald, W. L. Kruer, K. Tanaka, R. Betti, T. J. B. Collins, J. A. Delettrez, S. X. Hu, J. A. Marozas, A. V. Maximov, D. T. Michel, P. B. Radha, S. P. Regan, T. C. Sangster, W. Seka, A. A. Solodov, J. M. Soures, C. Stoeckl, and J. D. Zuegel. Direct-drive inertial confinement fusion: A review. *Physics of Plasmas*, 22(11):110501, November 2015. ISSN 1070-664X, 1089-7674. doi: 10.1063/1.4934714. URL <https://pubs.aip.org/pop/article/22/11/110501/109006/Direct-drive-inertial-confinement-fusion-A-review.10>
- [16] V N Goncharov, S P Regan, E M Campbell, T C Sangster, P B Radha, J F Myatt, D H Froula, R Betti, T R Boehly, J A Delettrez, D H Edgell, R Epstein, C J Forrest, V Yu Glebov, D R Harding, S X Hu, I V Igumenshchev, F J Marshall, R L McCrory, D T Michel, W Seka, A Shvydky, C Stoeckl, W Theobald, and M Gatu-Johnson. National direct-drive program on OMEGA and the National Ignition Facility. *Plasma Physics and Controlled Fusion*, 59(1):014008, January 2017. ISSN 0741-3335, 1361-6587. doi: 10.1088/0741-3335/59/1/014008. URL [https://iopscience.iop.org/article/10.1088/0741-3335/59/1/014008.10](https://iopscience.iop.org/article/10.1088/0741-3335/59/1/014008)

Permissions